Research Article

Experimental and Numerical Investigation into the Deep Drawability of DP500 Steel Sheet

A. Onur OZDEMIR[1],* , Murat DEMIRAL[2,3] , Cetin KARATAS[4] , Erhan KARA[5]

[1]Department of Automotive Engineering, Faculty of Technology, Gazi University, Ankara, Turkey
[2]Mechanical Engineering Department, University of Turkish Aeronautical Association, Ankara, Turkey
[3]College of Engineering and Technology, American University of the Middle East, Egaila, Kuwait
[4]Department of Manufacturing Engineering, Faculty of Technology, Gazi University, Ankara, Turkey
[5]İnegöl Technical Sciences Vocational School, Uludağ University, Bursa, Turkey

ABSTRACT

In today's automotive industry, the thick sheet materials used in the regions where safety is at the forefront have been replaced with thin and more durable sheets. Deep drawing has been widely used in their processing. The parameters affecting their formability quality need to be identified. In this study the appropriate corner radius value for the die entrance and the punch nose in the forming of the high strength dual-phase 500 steel sheets was determined. Initially, deep drawing tests were performed. Secondly, a three dimensional FE model of the process was developed. Forming Limit Diagram (FLD) damage initiation criteria accompanied by an appropriate damage evolution law was used to simulate the cracks formed in the samples in the course of deformation. The time history of the molding force, occurrence of the cracking and earing in the products as well as their thickness distribution for different tool geometries were predicted, and they were compared with those obtained experimentally.

Cite this article as: Onur O, Murat D, Cetin K, Erhan K. Experimental and Numerical Investigation into the Deep Drawability of DP500 Steel Sheet. Sigma J Eng Nat Sci 2021;39(3):237–247.

INTRODUCTION

Dual-phase (DP) steels produced from low or medium carbon steels have a microstructure predominantly composed by a soft ferritic matrix and hard martensite particles, where they ensure a good formability and higher strength, respectively. These properties make them favorable for automotive and other industries. Dual-phase steels are largely used in the components of a C-class car, designed with Advanced High Strength Steels approximately 85% of the body structure [1].

---

*Corresponding author.
*E-mail address: onurozdemir@gazi.edu.tr

This paper was recommended for publication in revised form by
Regional Editor Ayşegül Akdoğan Eker

Deep-drawing operation is used extensively in the forming of sheet metal into cup or box like structures. In that process, thickness of the sheet should remain as constant as possible for a successful forming. Punch speed, blank holder pressure, die clearance, tool edges and friction are the most important parameters influencing the quality of the drawn products [2]. In this complex process, fracture, wrinkling, thinning, tearing, necking, earing and spring back are mostly observed failure types due to very complicated deformation with tension, compression and bending loadings are applied simultaneously [3].

A few experimental and numerical studies were performed in the literature to investigate the deep drawing of DP steels. For instance, Song et al. showed that optimization of the blank holder and the draw-mold forces reduced the thickness variation of DP600 sheet material and ensured lower springback of the U-drawn formed canal pieces [4]. In another study, Liu et al. carried out deep drawing experiments and simulation at different blank holder forces to determine the forming property of an alloy sheet and to guide the process. They studied stress distribution and strain changes in deformation regions. Increased holder force has contributed to a reduction in ear formation [5]. Weld orientation did not affect the formability of DP600 at major strain direction; but, it had strong influence in DP980 laser welded blank. On the other hand, Bandyopadhyay et al. investigated the effect of laser welding on the formability of dual-phase steels and found that there was a decrease in

Erichsen cupping height compared to basis metals due to the softening in the heat affected areas of welded blanks [6]. Sung et al. using the draw-bend fracture test showed that the ratio of R to t, strain rate and the initial specimen width influenced the tensile failure, transitional failure and shear fracture of DP steels [7]. It was observed that deformation induced temperature also influenced the failure. For instance, increased strain rate promotes shear fracture because of the detrimental effect of deformation-induced heating in tight bending regions. Padmanabhan et al. investigated the influence of anisotropy in the stitch-welded sheet material on its formability with a numerical method [8]. It was observed that the punch force increased with the anisotropy due to the unequal metal flow in the sheets. Modanloo et al. have investigated various parameters, in order to achieve a successful thickness change in hydrodynamic deep drawing of a copper sheet material. It is determined that the high punch and die radius leads to a decrease in the thickness of the critical areas of the cup product [9]. A numerical model for forming operation of circular sheets was presented by Kadkhodaya. He found that the springback ratio trends to be lower in higher blanks. It was occurred less spring-back as using deformable tools [10]. Ossia and Soltani formed circular cups from AZ31B sheet and compared the numerical and experimental results of warm deep drawing. They showed that the limit drawing ratio rises with an increase in forming temperature. Also, they reported that an increment in punch speed causes a reduce in the drawing ratio limit.
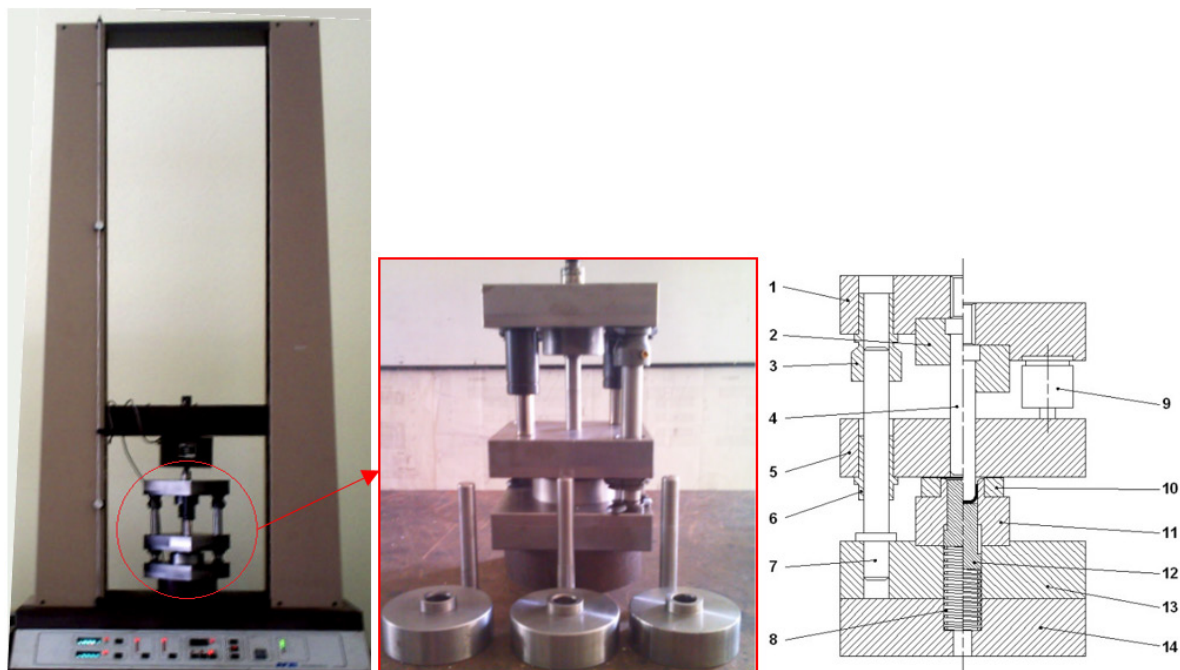

Figure 1. The universal test device and modular deep drawing set-up. (1.Top mold plate, 2.Punch holder plate, 3.Middle guide bush, 4.Punch, 5.Blank holder, 6.Top guide bush, 7.Middle guide pillar, 8.Mold spring, 9.Gas spring, 10.Stop pin, 11.Matrix, 12.Bottom thrust block, 13.Base mold plate, 14.Support plate)

It was concluded that increasing in the friction coefficient prompts to an increase in the punch force [11]. Forming limit curves were determined by experiments with eased Marciniak method. Experimental results played along with the new numerical method PEEQ (second time derivative of the equivalent plastic strain).

DP500 steel possesses good formability and weldability where it has been increasingly used in new generation automotive parts, especially for products where safety and security are required such as reinforcements. In none of the studies above, its formability was investigated thoroughly, especially in terms of size of the edge radius of the tools used. For this purpose, firstly, deep drawing tests of DP500 sheet was performed for different punch and die edge geometries. Secondly, a three dimensional FE model of the process was developed: An elasto-plastic material model with Forming Limit Diagram (FLD) damage initiation criteria was used to characterize the behaviour of the sheet material. To model the progressive failure, damage evolution option was activated. After validating the developed model based on the deep drawing force and thickness variation, the effects of tool edge geometries on the formability quality of the products were predicted.

EXPERIMENTAL PROCEDURE

In the deep drawing process, a 'blank' of sheet metal is clamped between a blank holder and a die. Then, a punch is moved against the blank to draw into the die.

In this study, the deep drawing experiments were carried out by using a set-up as shown in Fig. 1, where a designed modular die set was connected to the Hounsfield universal tensile/compression testing device. Its hydraulic power unit has a maximum load capacity of 50 kN, a displacement range of 1100 mm and an adjustable speed from 0.5 mm/min to 500 mm/min. A three-plate cross-column ready-made mold set was used for deep drawing to be on the same axis. Since three different edge radius values were used in the tests, three female molds and drawing punches were prepared. All mold elements were processed in Computer Numerical Control machine according to the required dimensional accuracy and surface quality, where the concentricity was taken into account during the assembly.

Table 1. Tool dimensions

Punch diameter, d_p (mm)	16
Inside die diameter, d_d (mm)	18.3
Punch nose radius, r_p (mm)	3-4-6
Die entrance radius, r_d (mm)	3-4-6
Blank holder inner diameter, d_h (mm)	18.3
Blank (sheet) diameter, D_b (mm)	32
Blank (sheet) thickness, t_b (mm)	0.9

The chemical composition of DP500 steel sheets studied here is as follows: 0.08 C, 1.205 Mn, 0.308 Si and 0.048 Al (wt %). Geometric dimensions of the parts used in the tests are given in Table 1. Here, three different sizes of corner radius of punch and die edges, namely 2 mm, 4 mm and 6 mm, were considered. It should be mentioned that same values were used for both corners at each test. The die clearance (c_d) was fixed at 1.15 mm following Eq. 1. While the punch diameter was 16 mm, that of the sheet metal was 32 mm to ensure that the limit drawing ratio (D_b/d_p) did not exceed 2 [12]. The thickness of steel sheets was 0.9 mm. Blank holder force was calculated to be 3770 N by using Eq. 2 and being applied in the tests [13]. All the deep drawn cups from the tests are shown in Fig. 2. They will be discussed more in detail in Section 4.

$$c_d = t_b + 0.07 \cdot \sqrt{10 \cdot t_b} \tag{1}$$

$$F_h = \left\{ \left[\left(\frac{D_b}{d_p} - 1 \right)^2 + \frac{d_p}{200 \cdot t_b} \right] \cdot \frac{\sigma_b}{400} \right\} \cdot \left(A_b - A_p \right) \tag{2}$$

NUMERICAL PROCEDURE

In this section the numerical methodology used in the simulations is presented. The analyses were performed using ABAQUS software. Fig. 3 is the developed Finite Element (FE) model of the deep drawing process for the DP500 steel. Owing to the symmetry, only one quarter of the process was simulated which ultimately reduce the computational time. Symmetry boundary conditions were applied as the x = 0 and z = 0 planes at the sheet quarter edges. The sheet material was considered deformable and modelled using continuum linear 4-node shell elements (S4R), where an enhanced stiffness-based hourglass and distortion control were employed. A mesh with element sizes of 0.5 mm × 0.5 mm was employed to discretize the workpiece material. The punch, die and holder were modelled using discrete rigid form, where they were meshed with R3D4 elements.

Simulations were carried out using explicit solver in a quasi-static manner. As a general rule the kinetic energy of

Figure 2. A view of the deep-drawn cups.

the deforming material should not exceed a small fraction (typically less than 10%) of its internal energy throughout the process [14]. In this analysis, the kinetic energy with a rate of 0.5% was found to be far less compared to the internal energy; hence confirming that possible dynamic effects onto the results are eliminated.

A general contact interaction property with kinematic constraint enforcement method for normal behaviour was utilised to model the contact between the punch, die, holder and the sheet material. Coulomb Friction Law was used for tangential motion with a coefficient of $\mu = 0.1, 0.01, 0.001$ for punch-sheet, die-sheet and holder-sheet interfaces, respectively.

The punch was allowed to move only in the z-direction and the die and the holder was fixed in all degrees of freedom to mimic the experiments. Eq. 3 is used to estimate the depth of the products to be obtained in the drawing process [15]. The ideal displacement (h) of the punch was calculated as 12 mm. However, to detect the maximum

Figure 3. The quarter symmetric FE model of the deep drawing process.

height and the earing texture, the punch was displaced up to 15 mm.

$$h = \frac{\left(D_b^2 - d_p^2\right)}{4 \cdot d_p} \qquad (3)$$

Elasto-plastic material model with FLD damage initiation criteria was used to characterize the behaviour of the sheet material. To model the progressive failure, damage evolution option was activated. The respective mechanical properties for DP500 were presented in Fig. 4 and Table 2. In the next, theory of the damage model used in the simulations is briefly explained.

The FLD described by the forming limit strains in the space of principal (in-plane) logarithmic strains is used to determine the amount of deformation that a material point can withstand before the failure starts [18]. In fact, major and minor limit strains refer to the maximum and minimum values of the in-plane principal limit strains, respectively with the former is represented on the vertical axis and the latter is on the horizontal axis. The forming limit curve (FLC), the line connecting the states at which deformation becomes unstable, gives a sense of the formability of a sheet of material [19].

The damage initiation criterion for the FLD used in the simulations is given by the following equation:

$$\omega_{FLD} = \frac{\varepsilon_{major}}{\varepsilon_{major}^{FLD}\left(\varepsilon_{minor}\right)} \qquad (4)$$

where ε_{major} is the current major principal strain and $\varepsilon_{major}^{FLD}(\varepsilon_{minor})$ is the major limit strain on the FLC evaluated at the current values of the minor principal strain. Fig. 5 represents the FLC curve for DP500 steel used in the simulations.

After the damage initiation criterion was achieved at any material point, displacement type damage evolution with linear softening law was used to describe the progressive damage of the material. Here, the effective plastic displacement, $\dot{u}$, is defined as $\dot{u} = l_e \dot{\varepsilon}$, where l_e is the characteristic length of the element and $\dot{\varepsilon}$ is the equivalent plastic strain rate. The damage variable ($\dot{d}$) changes according to the following equations:

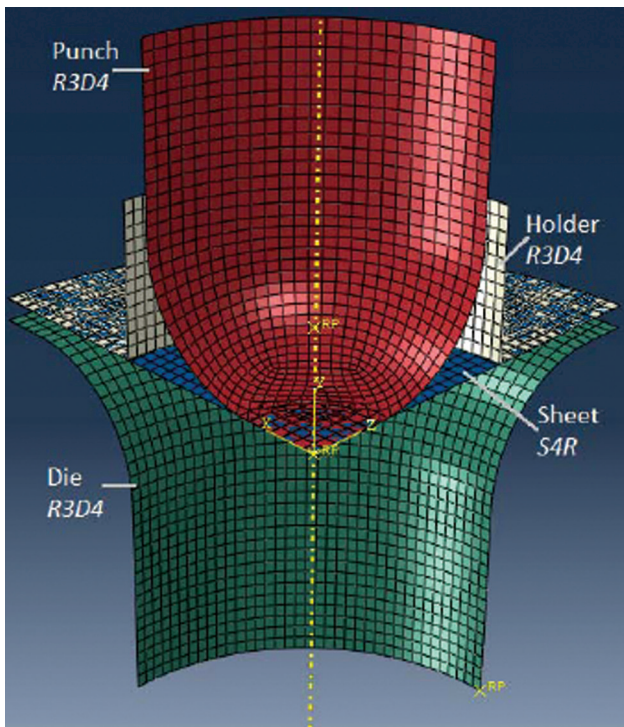$$\dot{d} = \frac{l_e \dot{\varepsilon}}{u_f} = \frac{\dot{u}}{u_f} \qquad (5)$$

Table 2. Typical mechanical properties of DP500 steel [16]

Material	Yield Stress (MPa)	Ultimate Tensile Strength (MPa)	Elongation at Break (%)	Density (kg/m³)	Young's Modulus (GPa)	Poisson's Ratio
DP500	390.0	660.0	0.178	7850	210	0.3
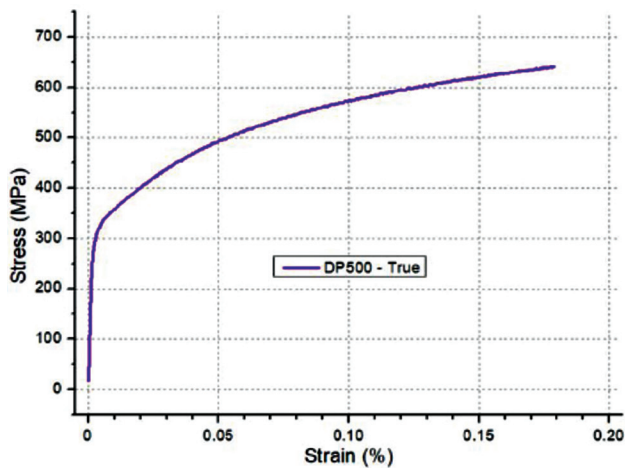
Figure 4. True tensile stress-strain curves for DP500 steel [17].

Figure 5. Forming Limit Diagram for DP500 steel [20].

where u_f is the effective plastic displacement at failure and the material stiffness is fully degraded when u_f reaches this constant value. It was specified to be 0.1 in the current study.

RESULTS AND DISCUSSION

In this section, the effect of edge corner radius of punch and die on the formability of the DP500 steel was investigated thoroughly in terms of the evolution of the force applied, change in the thickness of the sheet material, crack initiation and its evolution and occurrence of the earing. In the graphics; '*R-*', '*Num.*' and '*Exp.*' stand for the tool corner radius, numerical and experimental results, respectively.

Fig. 6 demonstrates the obtained molding force-displacement curves for different radius value, i.e. 2.2 mm, 3 mm, 4 mm, 4.9 mm and 6 mm. For the first and fourth cases only the numerical results are presented. The molding force value here is the sum of the force holding the specimen and the punch force forming the sheet material. A reasonably good agreement between them was achieved. It was observed that with an increase in the tool radius, the molding force decreased, but the penetration depth at which the peak force was obtained increased. This can be explained by the fact that for a smaller corner radius value of the punch, the sheet is kept tightly by its corners and the contacted respective regions are deformed significantly. Consequently, the maximum force value is reached at lower depth just before the crack initiates in these corner regions. On the other hand, when a tool with a larger radius value is used, the workpiece material can not be squeezed from its corners, hence the deformation is not restricted to a local region, but to a larger region including the base
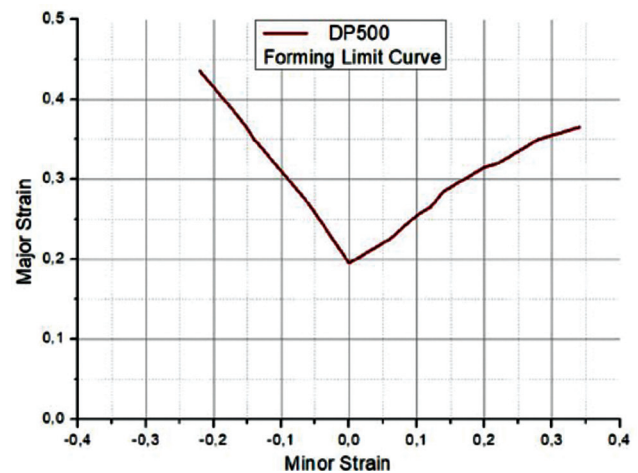
part. Therefore, the crack initiation is delayed and the maximum force is reached at far depths. As the surface area of the punch contacting the workpiece with a normal angle is larger in the former case, a larger molding force is observed. Consequently, the wear in the tools is expected to be severe compared to the second case. Parallel observations were reported in Gowtham et al. and Mansourinejad et al. [21, 22]. Aydin et al. measured that the forces increase with raising the cup depths [23].

In the deep drawing process, the wall thickness should be kept under control to satisfy the dimensional accuracy of the parts produced. In fact after the initial contact of the punch to the sheet, with its penetration, bending stresses occurring on the sheet have tensile and compressive characteristics. Also, due to the frictional forces developed tensile and bending stresses occur in the non-contact zones. As the punch progresses into the mold, only tensile stresses play an active role in the sheet material within the mold. Consequently, regional differences are observed in the wall thickness of the products [24]. Experimentally and numerically obtained percentage thickness variation along one of the axes of the drawn product for different corner radius values are presented in Fig. 7. In this figure section points between -3 to 3 represent the base, –3 to –5 and 3 to 5 the corners, –5 to –7 and 5 to 7 the side walls. A noticeable matching between them was achieved. Since the number of data points taken in the experiments were limited, numerically obtained variations were not observed. It was numerically noted that the thinnings in the base region of the workpiece were 3%, 4%, 6% and 8% when the edge radius of 3 mm, 4 mm, 4.9 mm and 6 mm were used, respectively. The respective maximum thinning in the corner regions were calculated as 14%, 12% and 11% and 12%. On the other hand, the maximum
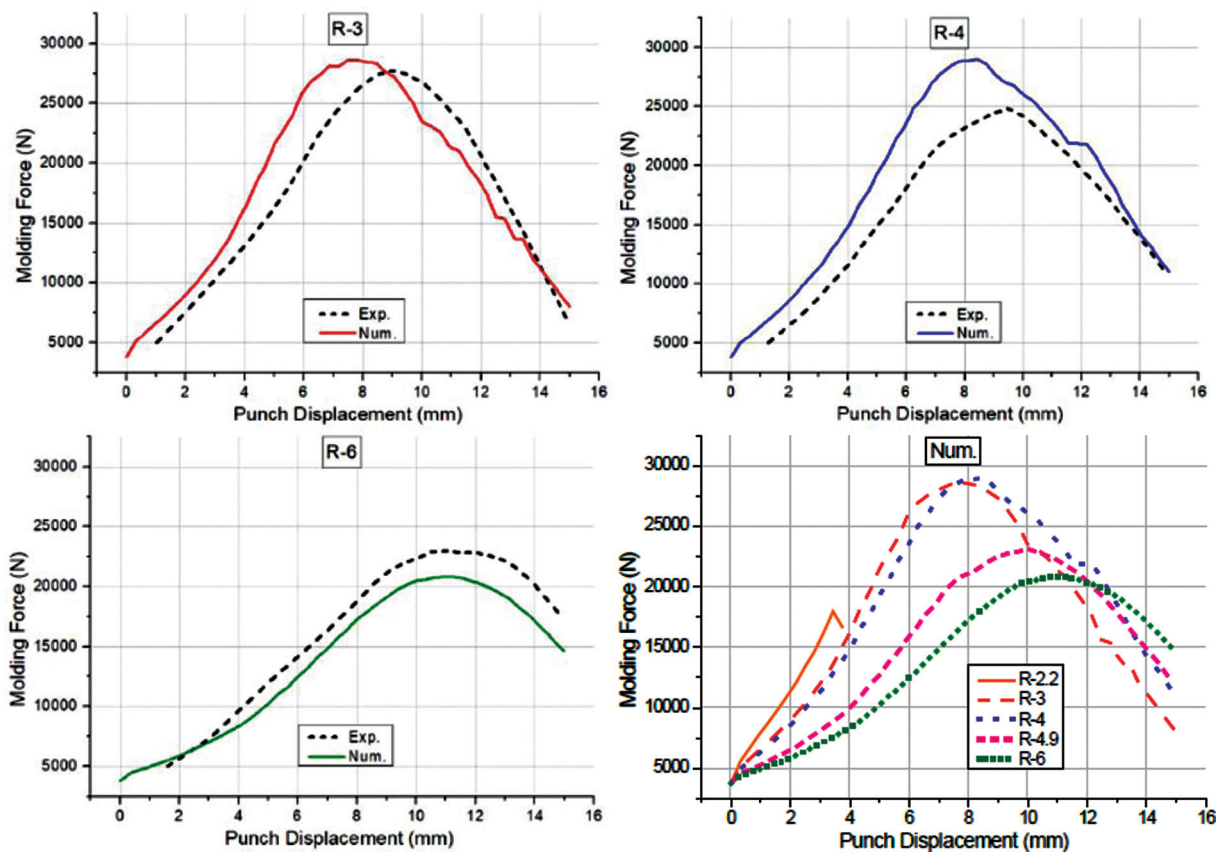
Figure 6. Experimentally and numerically obtained molding force vs. punch displacement plots for different tool edge radius values.

thickenings at the top part of the products are 36%, 34%, 30% and 26%, respectively. For a punch with a smaller edge radius, the workpiece material is caught firmly from its corners, hence, the side walls are deformed significantly followed by a thinning, whereas this is very limited in the base region. Ultimately, the thickness of the product base is about the initial thickness of the material. As the radius increases, the region of the sheet material contacted by the punch with an angle increases, hence the deformation was well distributed in the sample resulting in some thinning in the base material. In parallel, Ziaeipoor et al. and Zein et al. reported in their studies that thinning on corners of the workpiece reduced with an increase in the die shoulder radius and using a greater punch nose radius [25, 26].

It was numerically observed that the failure occurred in the regions in contact with the corners of the punch for its radius value of 2.2 mm (Fig. 8). In the course of deformation, when the thickness fell below 79% of its initial value at a depth of 3.125 mm (see Figs. 9 and 10), the damage initiated, i.e. the cracks began to arise, and ultimately the tearing occurred when the minimum thickness variation reached to 63% (see Fig. 8).

Fig. 9 demonstrates the distribution of percent change in the thickness of sheet material for different tool edges. For larger tool radius, for example in the case of R-4.9 and R-6, a more homogeneous distribution with less thickening and thinning was obtained. For the second one, however, the thinning occurred in the base region were severe (see also Fig. 8). It was therefore concluded that R-4.9 was the optimum tool geometry among those studied for the deep drawing of DP500.

The effects of tool geometry on the height of the drawn products and occurrence of earing were predicted. The beginning of the shoulder at the top of the piece represents the minimum height, while the peak point is the maximum, and the difference in between considered as the earing as shown in Fig. 10. It was noted that the regions parallel to the rolling and transverse directions had the minimum heights while those with ±45° w.r.t these directions had the maximum values. It was observed that with an increase in the tool corner radius, the maximum height of the formed workpiece was increased, whereas the tendency of the earing formation was reduced. Similar results were reported in Bouchaala et al. [27]. It was shown above that a larger surface area was exposed to the thinning with the tools having
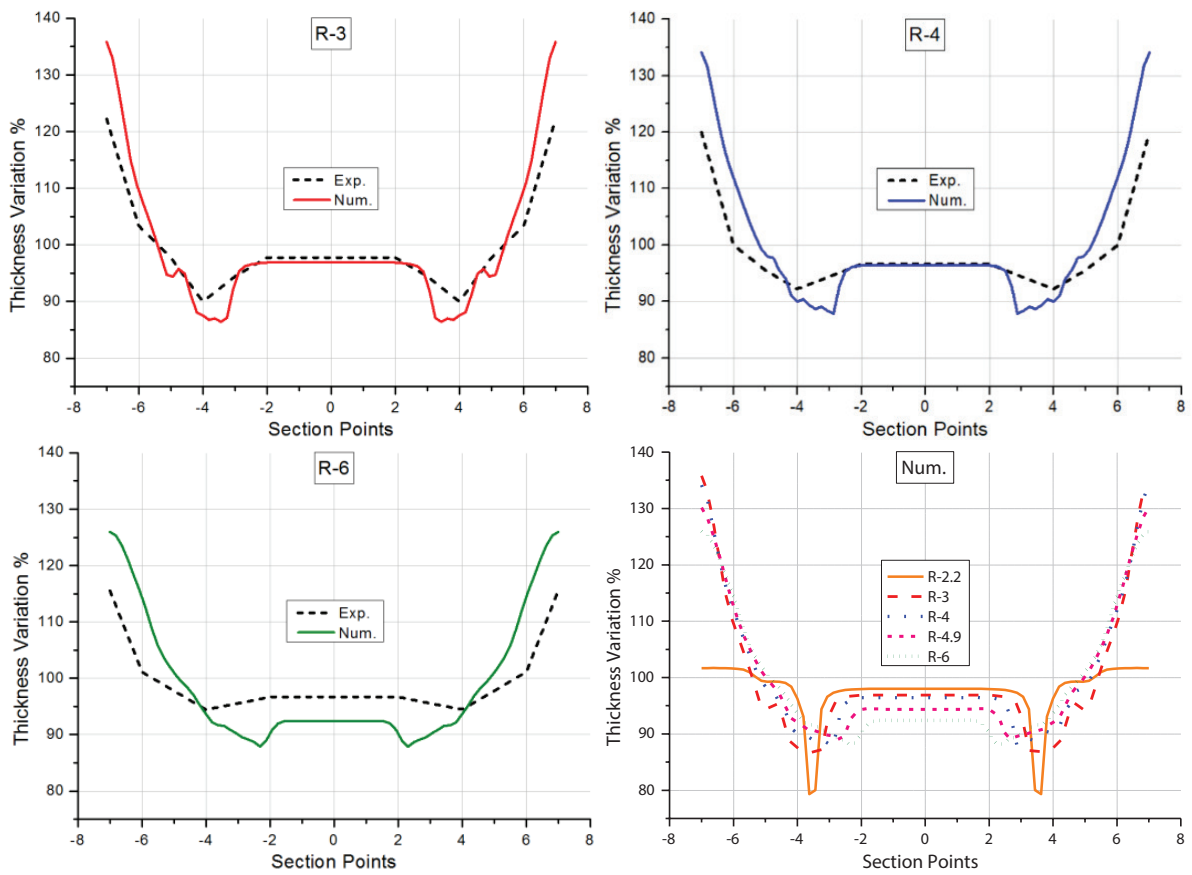
Figure 7. Comparison of the percentage thickness distributions of drawn products along with one of the axes for different tool geometries.
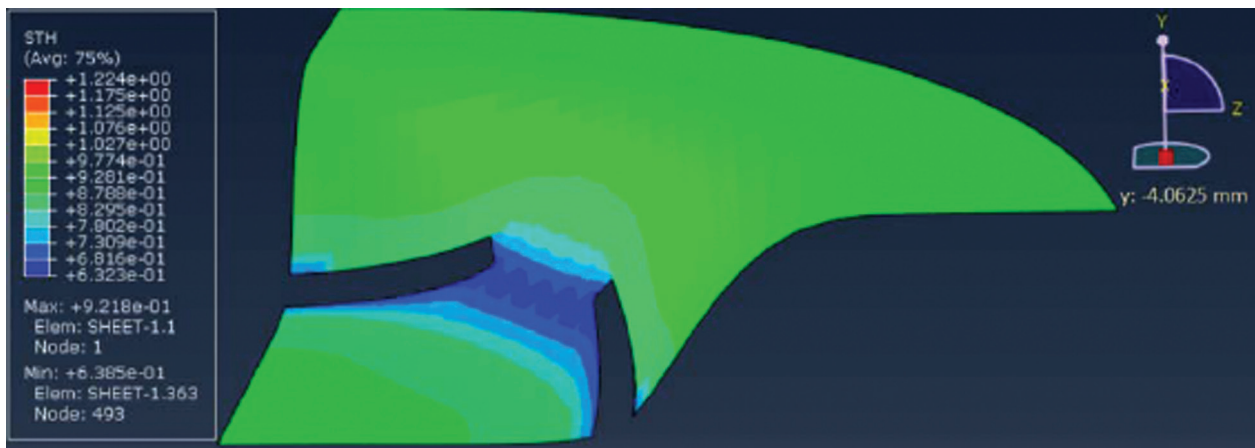

Figure 8. Distribution of unit thickness change of the sheet material when R-2.2 was used.

a larger edge corner radius. In fact, material volume in these regions flew upward direction and hence the earing formation was reduced. Before the drawn products are used in the service, they should be cut circumferentially from the minimum height level to eliminate the earing formed, therefore their height are shorter than the desired. Ear formation, therefore, should be minimized since it causes loss of material and increases the cost with an additional cutting step.

In a deep drawing procedure, the risk of failure can be evaluated by using the FLD defined in the plane of principal
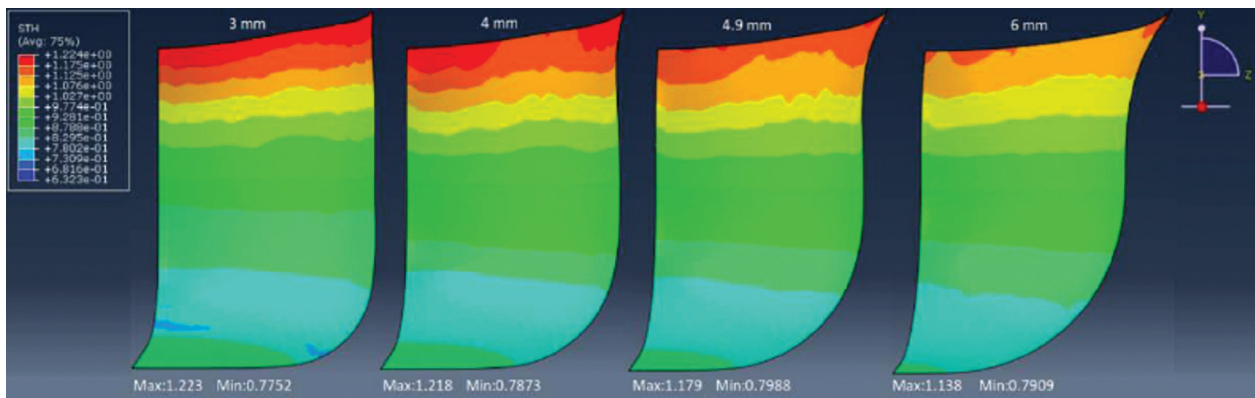
Figure 9. Distribution of unit thickness change of the sheet material when the corner radius of 3 mm, 4 mm, 4.9 mm, and 6 mm for the tool edges were used.
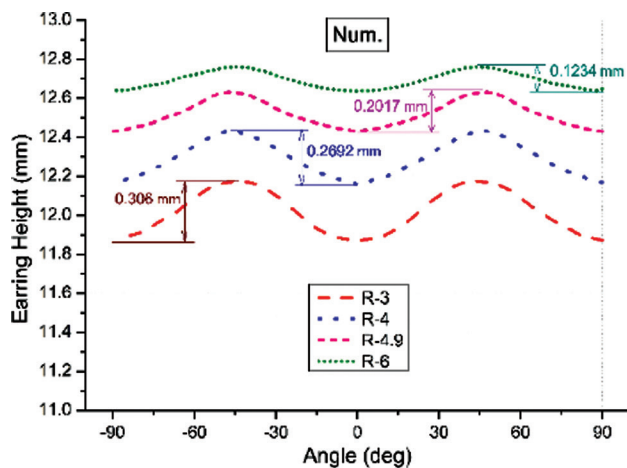

Figure 10. Predicted earing profile of the drawn products vs. rolling direction at various tool edge radius values.
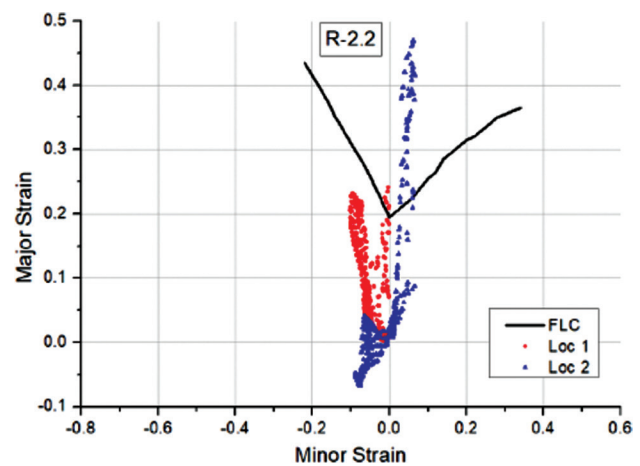

Figure 11. Comparison of forming limit curve with major vs. minor strain values for different material points of the workpiece material when R-2.2 was used.

strains [28]. Here, we compared the predicted in-plane major and minor strains with the forming limit curves. Fig. 11 demonstrates the corresponding values for the corner edge radius value of 2.2 mm. In this figure, Loc 1 and Loc 2 refer to the different integration points of a shell element with the fractions of –0.774597 and 0.774597 lying on the SNEG and SPOS surfaces, respectively, at which values are calculated [19]. It was seen that the damage occurred at both surfaces of some elements in the sheet material since the intersection of principal values (shown as dots) are above the FLC. Of them, Locs 1 and 2 had a compressive and tensile characteristics, respectively due to the bending effect. When the scalar damage variable showing the degree of damage level reached unity, complete failure reached and the corresponding elements were removed from the FE mesh (Fig. 8).

Fig. 12 presents the plots of principal strains for other tool geometries. It is known that the points indicated by the

red (or round shape) and blue (or triangular shape) colors represent the region in the proximity of the inner and outer surface, respectively. The respective regions were exposed to compressive and tensile loadings as a consequence, they were getting thicker and thinner. In the case of R-3 and R-4, some material points exposed to tensile stresses were beyond the safe zone. However, there was no crack initiation and propagation with regards to these elements was observed since not all the integration points of these elements exceed the FLC.

Filho and Marcondes reported that in the case of smaller tool edge radius was used, the major strains occurred significantly in the region contacted with die shoulder and surface of the punch [29]. Risk of tearing was reduced for larger corner radius value. As seen in Fig. 12 for the cases of R-4.9 and R-6, the principal strain values at none of the integration points exceed the critical region, hence the damage initiation does not take place.
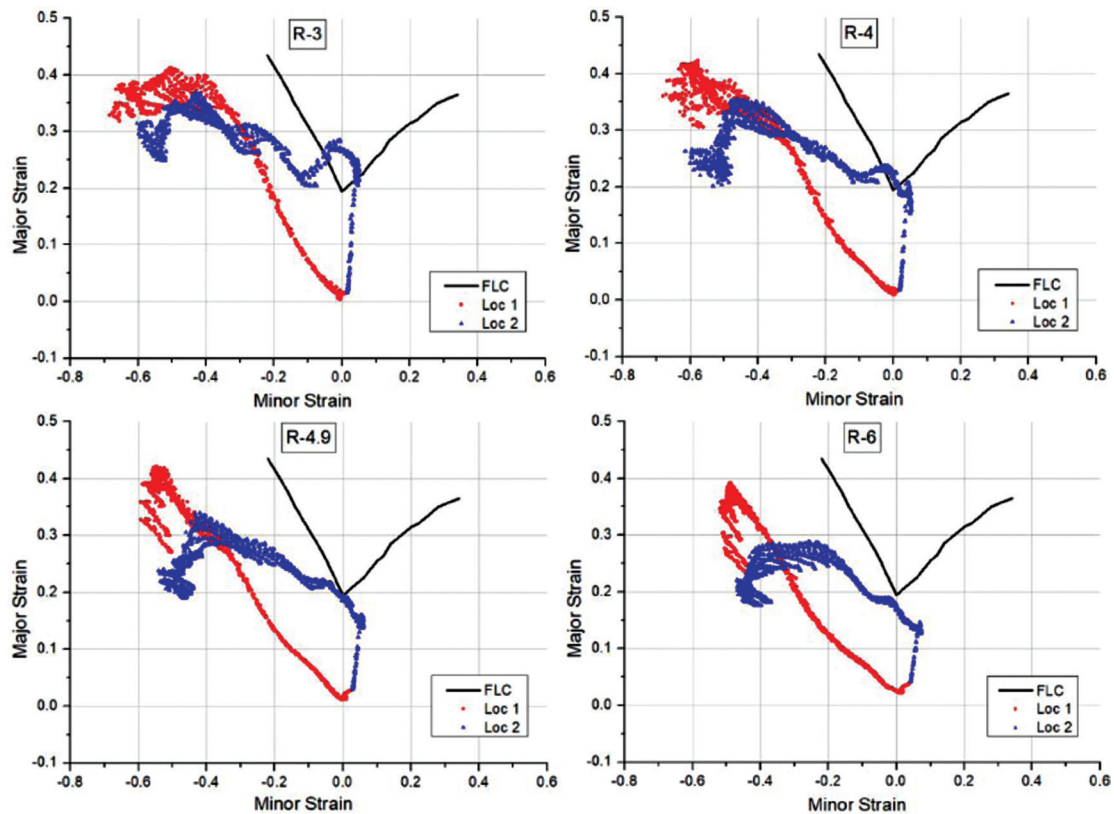
Figure 12. Comparison of forming limit curve with major vs. minor strain values for different material points of the work-piece material when different tool geometries were used.

CONCLUSION

In this study, the deep drawing of the DP500 steel sheet was investigated both experimentally and numerically. In the developed FE model, the crack initiation in the sheet material in the course of deformation was predicted using the Forming Limit Diagram (FLD) damage initiation criteria.

From our study, the following observations and conclusions were made:

- It was observed that the corner radius value of die entrance and punch nose had strong effects on the drawn products.
- With an increase in the corner edge radius value of the tools, the deformation in the products was well distributed, therefore, a more homogeneous thickness distribution (with less thickening and thinning) was achieved. At the same time, their maximum height was increased, but the tendency of the earing formation was reduced. In parallel, the wear in the tools was expected to be less since a smaller maximum force was reached at far depths.
- The tools with a corner edge radius value of 2.2 mm caused tearing in the forming of DP500 sheet material

having an initial thickness of 0.9 mm. That of 4.9 mm was found to be the optimum tool geometry.
- FLDs were used to predict the drawability of the products with different tool geometries. It was observed that the damage initiated at the material points of an element exposed to tensile loading rather than the compressive one.

NOMENCLATURE

A_b	Sheet area (m^2)
A_p	Punch area (m^2)
c_d	Die clearance (mm)
D_b	Sheet diameter (mm)
d_b	Punch diameter (mm)
d	Damage variable
F_h	Blank holder force (N)
l_e	Element characteristic length
h	Punch displacement (mm)
t_b	Sheet thickness (mm)
u_f	Effective plastic displacement at failure
$\dot{u}$	Effective plastic displacement
σ_b	Sheet tensile strength (MPa)
ω	Damage initiation criterion
$\varepsilon_{major}^{FLD}$	Current major principal strain

$\varepsilon_{major}^{FLD}\,(\varepsilon_{minor})$ Major limit strain as a function of minor limit strain

$\dot{\varepsilon}$ Equivalent plastic strain rate

AUTHORSHIP CONTRIBUTIONS

Concept: A.O.O., C.K.; Design: A.O.O.; Materials: E.K., C.K.; Data: A.O.O.; Analysis: A.O.O., M.D.; Literature search: A.O.O.; Writing: A.O.O., M.D.; Critical revision: A.O.O, C.K.

DATA AVAILABILITY STATEMENT

No new data were created in this study. The published publication includes all graphics collected or developed during the study.

CONFLICT OF INTEREST

The author declared no potential conflicts of interest with respect to the research, authorship, and/or publication of this article.

ETHICS

There are no ethical issues with the publication of this manuscript.

REFERENCES

[1] Zuidema BK, Denner SG, Engl B, Sperle JO. New high strength steels applied to the body structure of ULSAB-AVC, SAE Technical Papers 2001-01-3042, 2001. [CrossRef]

[2] Gusel L, Boskovic V, Domitner J, Ficko M. Genetic programming method for modelling of cup height in deep drawing process. Advances in Production Engineering & Management 2018;13:358–65. [CrossRef]

[3] Singh CP, Agnihotri G. Study of deep drawing process parameters: a review. International Journal of Scientific and Research Publications 2015;5:2250–3153.

[4] Song JH, Huh H, Kim SH. Stress based springback reduction of a channel shaped auto body part with high strength steel using response surface methodology. Journal of Engineering Materials and Technology 2007;129:397–406. [CrossRef]

[5] Liu ZY, Xiong BQ, Li XW, Yan LZ, Li ZH, Zhang YA, Liu HW. Deep drawing of 6A16 aluminum alloy for automobile body with various blank-holder forces, Rare Metals 2019;38:946–53. [CrossRef]

[6] Bandyopadhyay K, Panda SK, Saha P. Prediction of formability of laser welded dual phase steel by finite element analysis. Proceedings of the Institution of Mechanical Engineers. Part B: Journal of Engineering Manufacture 2014;228:1048–57. [CrossRef]

[7] Sung JH, Kim JH, Wagoner RH. The draw bend fracture test and its application to dual phase and transformation induced plasticity steels. Journal of Engineering Materials and Technology 2012;134:1–15. [CrossRef]

[8] Padmanabhan R, Baptista AJ, Oliveira MC, Menezes LF. Effect of anisotropy on the deep drawing of mild steel and dual phase steel tailor welded blanks, Journal of Materials Processing Technology 2007;184:288–93. [CrossRef]

[9] Modanloo V, Gorji A, Jooybari MB. A comprehensive thinning analysis for hydrodynamic deep drawing assisted by radial pressure, Iranian Journal of Science and Technology Transactions of Mechanical Engineering 2019;43:487–94. [CrossRef]

[10] Kadkhodayan M. An investigation into the influence of deformable dies on the springback of circular plates, Scientia Iranica 2006;13:201–5.

[11] Ossia SA, Soltani B. Finite element simulation of the warm deep drawing process in forming a circular cup from magnesium alloy sheet. Scientia Iranica 2013;20:1213–20.

[12] Bozdok M. Advanced high strength steel product and process, AHSS Applications Guidelines, Auto Steel Partnership, Michigan, 2008. Available at: https://www.worldautosteel.org/steel-basics/automotive-advanced-high-strength-steel-ahss-definitions/

[13] Tschaetsch H. Metal forming practise, Vieweg Verlag, Wiesbaden, 2005.

[14] Poor HZ, Moosavi H. An investigation of wrinkling and thinning in hydroforming deep drawing process with hemispherical punch. International Journal of Mechanic Systems Engineering 2019;3:89–96.

[15] Güneş AT. Pres işleri tekniği, Cilt 2, Chamber of Mechanical Engineers, Ankara/Turkey, 2005.

[16] Liao J, Xuea X. Experimental investigation of deep drawing of C-rail benchmark using various lubricants, 4th International Conference on New Forming Technology, Scotland/UK, 2015:1–6.

[17] Cornette D, Hourman T, Hudin O, Laurent JP, Reynaert A. High strength steels for automotive safety parts, SAE Technical Paper 2001-01-0078, 2001 [CrossRef]

[18] Keeler SP, Backofen WA. Plastic instability and fracture in sheets stretched over rigid punches, ASM Transactions Quarterly 1964;56:25–48.

[19] Abaqus, User's Manual, Documentation Version 6.13, Dassault Systemes, Providence/RI, 2013.

[20] Mittal A. Dual phase steels, extract from the product catalogue. Automotive Worldwide 2018

[21] Gowtham K, Srikanth KVNS, Murty KLN. Simulation of the effect of die radius on deep

drawing process. International Journal of Applied Research in Mechanical Engineering 2012;2:2231–5950. [CrossRef]

[22]   Mansourinejad M, Mirzakhani B, Pishbin H, Amadeh A. Influence of die and punch profile radii on deep drawing force and punch load displacement diagram, International Conference on Advances in Materials and Processing Technologies, France. 2011:389–94. [CrossRef]

[23]   Aydin M, Wu X, Cetinkaya K, Yasar M, Kadi I. Application of digital image correlation technique to erichsen cupping test. Engineering Science and Technology an International Journal 2018;21:760–8. [CrossRef]

[24]   Çınar G. Effects of anisotropy on formability in sheet metal forming. Master Thesis: Istanbul: Istanbul Technical University, 2006.

[25]   Ziaeipoor H, Moosavi H, Menghari HG, Sousa RJA. Investigation of punch nose radius and punch-die clearance on thinning and puckering in hydro mechanical deep drawing process, International Journal of Mechanic Systems Engineering 2014;4:16–21.

[26]   Zein HLE, Abdrabou M, Elsherbiny M, Shazly M. Effect of die design parameters on thinning of sheet metal in the deep drawing process, American Journal of Mechanical Engineering 2013;1:20–9. [CrossRef]1

[27]   Bouchaala K, Essadiqi E, Mada M, Ghanameh MF. Prediction of earing in cylindrical deep drawing of aluminum alloys using finite element analysis. Academics World International Conference, Rabat/Morocco 2018:1–7.

[28]   Ramos GC, Stout M, Bolmaro RE, Signorelli JW, Serenelli M, Bertinetti MA, et al. Study of a drawing quality sheet steel II: Forming limit curves by experiments and micromechanical simulations. International Journal of Solids and Structures 2010;47:2294–9. [CrossRef]

[29]   Filho RAC, Marcondes PVP. True strain distribution profile on sheet metal using different punch geometries. The Journal of the Brazilian Society of Mechanical Sciences and Engineering 2008;30:1–6. [CrossRef]